# A Differential Scanning Calorimetry Study of the Crystallization Kinetics of Tristearin-Tripalmitin Mixtures

**W. MacNaughtan[a], I.A. Farhat[a], C. Himawan[b], V.M. Starov[b], and A.G.F. Stapley[b,*]**

[a]Division of Food Sciences, University of Nottingham, Nottingham, United Kingdom, and
[b]Department of Chemical Engineering, Loughborough University, Loughborough, United Kingdom

**ABSTRACT:** A comprehensive study of the isothermal crystallization kinetics of tripalmitin-tristearin mixtures was carried out using DSC, with data fitted to the Avrami equation. Polymorphs were identified by subsequent melting of samples in the differential scanning calorimeter, with additional confirmatory information obtained from wide-angle X-ray diffraction. It was found that α-, β′-, and β-forms require small (<1.0°C), moderate (3.5–8.5°C), and large (9.0–13.0°C) amounts of subcooling below their respective polymorph melting temperatures for nucleation to occur. Concurrent crystallization of β and β′ polymorphs was not observed. The β polymorphs exhibited sharper heat flow exotherms than β′, due to the higher crystallization driving forces experienced. Analysis of apparent induction times shows that the activation free energy of nucleation for the β-form is significantly higher than for the β′-form. Samples rich in either species crystallized faster (both shorter apparent induction times and sharper peaks) than samples with equivalent compositions. Driving-force arguments do not fully explain this behavior, strongly suggesting that mass transfer resistances (greatest for equivalent compositions) have a significant effect on kinetics. Multiple crystallization events were observed for 50–80% tristearin samples between 56 and 60°C and were attributed to a demixing of tripalmitin-rich and tristearin-rich β phases, in line with established phase diagrams.

Paper no. J11158 in *JAOCS 83*, 1–9 (January 2006).

**KEY WORDS:** Avrami, crystal growth, driving force, DSC, induction time, melting, nucleation, polymorphism, triglyceride, X-ray diffraction.

The phase behavior and crystallization kinetics of TG have been extensively studied (1), and these studies have generally concentrated on either single TG or natural fats. Natural fats are complex multicomponent mixtures of TG and other minor components, and their crystallization behavior is poorly understood in comparison with well-defined systems of pure TG. A better understanding is required. One approach to the behavior of real fats is to build up an understanding of the interactions between individual TG components. A number of workers have studied the equilibrium phase behavior of mixed TG, and this has resulted in the publication of phase diagrams for a number of binary and ternary systems (2,3). Much rarer, however, are studies where the crystallization kinetics of mixed systems are examined (4,5). This paper seeks to study such behavior in tripalmitin-tristearin binary mixtures.

The polymorphic and phase behavior as well as the crystallization kinetics of pure tripalmitin and tristearin has been reported previously in the literature (6–10). However, relatively few studies have been performed on blends of tripalmitin and tristearin, although a phase diagram is well established (11–13). In this work, the isothermal crystallization and subsequent melting of tripalmitin-tristearin mixtures covering the whole composition range were studied using DSC. This technique is able to provide accurate and reproducible kinetic data and also yields information on the identity of the resulting polymorphs by a subsequent melting of the crystallized material, which can be compared with literature data (14,15). However, DSC does not always provide unequivocal identification of polymorphic forms, especially in blends containing species of different melting points. X-ray diffraction was used to resolve ambiguous cases of polymorph identity.

The aim of these experiments was to investigate thoroughly the effect of composition and isothermal temperature on the polymorphic behavior and the crystallization kinetics of these mixtures. It is hoped that such an approach will contribute to a better understanding of real fat systems.

## MATERIALS AND METHODS

*Materials.* All materials were used as supplied without further purification. Tripalmitin and tristearin were obtained from the Sigma Chemical Co. (>99% pure; Dorset, England). Samples were formulated at intervals of 10% composition on a mass basis and were weighed directly into the DSC pans. Stainless steel pans were used, as they were found to give more reproducible results in preliminary experiments compared with aluminum pans. This may be due to the larger mass used for the stainless pans, which increases the chance of consistent numbers of nuclei being present.

*DSC.* The calorimeter used was a PerkinElmer Pyris Diamond equipped with an autosampler. Calibration for temperature was carried out using indium and cyclohexane, and for enthalpy using indium. Calibrations were applied for a 10°C $min^{-1}$ scanning rate (16). This was then corrected for isothermal conditions by adding a value of 0.5°C to all recorded sample temperatures, which corresponds to the difference between a calibration at 10°C $min^{-1}$

*To whom correspondence should be addressed at Dept. of Chemical Engineering, Loughborough University, Ashby Road, Loughborough, Leicestershire, LE11 3TU, United Kingdom. E-mail: A.G.F.Stapley@lboro.ac.uk

and a calibration extrapolated to zero scan rate, obtained from a series of calibrations performed at different scan rates.

After loading into the DSC, samples were first heated to 90°C and held for 5 min to obtain an isotropic melt and to melt potential high m.p. impurities. Thereafter the sample was cooled at a rate of 50°C $min^{-1}$ to an isothermal holding temperature in the range 50.5 to 62.5°C for tristearin-rich samples or 40.5 to 62.5°C for tripalmitin-rich samples. Samples were then held at the isothermal holding temperature for times ranging from 20 to 90 min. During this time, crystallization was monitored by observing the isothermal heat flow. The sample was then heated at a rate of 10°C $min^{-1}$ to 90°C to provide a melting endotherm for polymorph identification by comparison with the melting temperature of peaks from the literature (2,3,11). Samples were reused for further experiments by holding for 3 min at 90°C before once again cooling to a second isothermal temperature. Preliminary experiments suggested that continual reheating of samples had little effect on their melting and crystallization behavior, which is not unexpected as these lipids are saturated and thus relatively unreactive. Thus, all thermograms relating to a specific composition are based on the same sample.

*X-ray diffraction.* The X-ray measurements were carried out using copper Kα radiation of wavelength 1.54 Å on a Bruker model D5005 X-ray diffractometer operating in θ/θ mode and equipped with an Anton Paar variable temperature stage. Rapid cooling (up to 30°C $min^{-1}$) and heating of samples was achieved by a jet of liquid nitrogen directed onto a cold finger assembly together with direct electrical heating of the sample holder. Temperature control was accurate to within 1°C. Condensation problems on the sample were avoided by purging the sample chamber with dry gas or pulling a vacuum line on the system. Accurate calibration of the diffraction angle was obtained by using silicon powder as a standard.

*Data treatment.* The DSC crystallization data were fitted to the Avrami equation (17,18) supplemented by an apparent induction time; see Equation 1. This was applied to the DSC traces after subtracting the baseline and normalizing by dividing by the total peak enthalpy.

$$X_{\text{solid}}(t) = 1 - \exp[k(t - t_{\text{ind}})^n] \quad [1]$$

The fitted parameters are $k$, a rate constant; $n$, a geometric factor; and $t_{\text{ind}}$, the apparent induction time; and $X_{\text{solid}}(t)$ is the solid fraction of the sample at time $t$. The parameter $k$ is related to the growth rate of crystals, but the units of $k$ are dependent on $n$. Therefore, to provide a better indicator of the relative rates of crystallization post-nucleation, a composite variable was defined, $t_{1/2}$, which is equivalent to the time taken for half of the overall level of crystallization to be reached after the apparent induction period has passed, or

$$t_{1/2} = \left(\frac{\ln 2}{k}\right)^{1/n} \quad [2]$$

Parameter estimations were performed using the curve-fitting toolbox in MATLAB® 7 (Mathworks, Inc., Natick, MA). For data exhibiting a very long apparent induction time, it was often necessary to assist the curve-fitting algorithm by providing an allowable range for $t_{\text{ind}}$. This was achieved in practice by manually truncating the start of the dataset, performing the fit, and adding the truncated time back to the fitted time to give the recorded induction time. It should be emphasized that the apparent induction times quoted are the results of fits of the entire crystallization curve to the Avrami equation, and are not based on the first detectable signs of crystallization, which is common in many studies of nucleation. The accuracy of the apparent induction times quoted is thus more dependent on the ability of the Avrami equation to model the crystallization realistically than the sensitivity of the technique to detect crystal nuclei. Reproducibility studies by which three repeat scans were made of the same experiment were performed on selected samples.

The induction time of nucleation is often assumed to correlate inversely with the nucleation rate $J$ (although they refer to two different aspects of nucleation). The nucleation rate can be related to the activation free energy of nucleation, $\Delta G_{\text{cryst}}$, by the Fisher–Turnbull equation (19):

$$J = \frac{Nk_BT}{h}\exp\left(\frac{-\Delta G_{\text{diff}}}{k_BT}\right)\exp\left(\frac{-\Delta G_{\text{cryst}}}{k_BT}\right) \quad [3]$$

where $\Delta G_{\text{diff}}$ is the activation energy of diffusion; $k_B$ is the Boltzmann constant; $N$ is the Avogadro number; $h$ is Planck's constant; and $T$ is the absolute temperature. The activation free energy of nucleation is related to the surface free energy of the crystal/melt interface, σ, and the crystallization temperature driving force $\Delta T$. We have defined $\Delta T$ as the degree of subcooling below the m.p. of the polymorph that forms $T_p$, i.e., $\Delta T = (T_p - T)$. If spherical nuclei are assumed this expression gives (20):

$$\Delta G_{\text{cryst}} = \frac{16}{3}\pi\sigma^3\frac{\left(T_p\right)^2}{\left(\Delta H_{\text{cryst}}\right)^2\left(\Delta T\right)^2} \quad [4]$$

Consequently, a plot of $\ln(Tt_{\text{ind}})$ vs. $1/T(\Delta T)^2$ allows calculation of the activation free energy of nucleation from the slope, $s$, using the following equation (20):

$$\Delta G_{\text{cryst}} = \frac{sk_B}{\left(T_p - T\right)^2} \quad [5]$$

## RESULTS AND DISCUSSION

The DSC isothermal crystallization and remelting curves for pure tripalmitin, tristearin, and their mixtures are shown in Figures 1–3. The phase diagram for a mixture of tripalmitin and tristearin from reference (11) obtained *via* capillary melting experiments, as well as that reconstructed from the melting curves in this work, is presented in Figure 4. Table 1 summarizes the results of the Avrami fits (including $t_{\text{ind}}$ and $t_{1/2}$) and also shows the polymorphic occurrence; the driving force for crystallization, which is defined as the degree of subcooling below the m.p. of

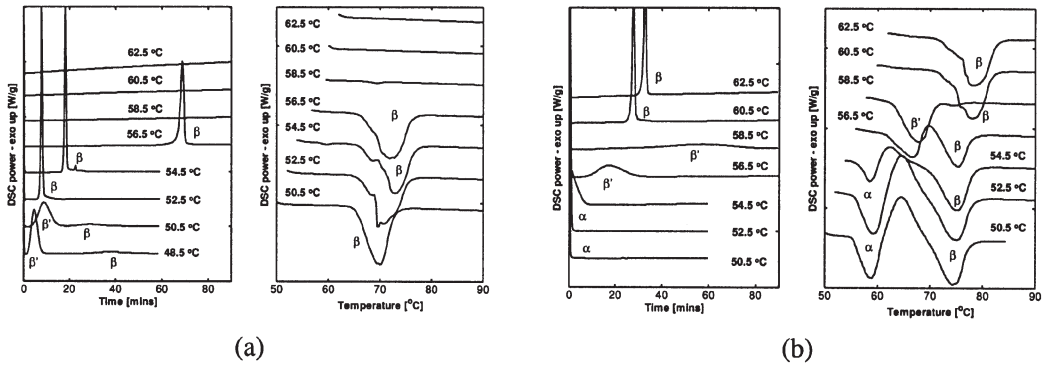


**FIG. 1.** DSC thermograms showing isothermal crystallization and melting of (a) pure tripalmitin and (b) pure tristearin. The y-axis scale divisions for crystallization and remelting thermograms are 1.0 and 10 W/g, respectively.

the crystallizing polymorph ($T_p - T$); the peak enthalpies; and the goodness of fit represented by the root mean square of error (RMSE).

*Polymorphic occurrence.* Within the timeframe and temperatures used, the β-form was observed at the higher isothermal hold temperatures (52.5–56.5°C for tripalmitin–rich and 58.5–62.5°C for tristearin-rich samples), but no β form was observed with 30 and 40% tristearin samples (see Table 1). The β′ polymorph formed preferentially below these temperatures in a band running from 44.5 to 50.5°C for tripalmitin and 56.5 to 58.5°C for tristearin. Temperatures below this band lead to the formation of the α polymorph, although there is some overlap with β′. The observed crystallization enthalpies lie between 140–170 and 162–192 kJ/kg for β′- and β-forms, respectively.

Table 1 also shows that the α-, β′-, and β-forms typically require small (<1.0°C), moderate (3.5–8.5°C), and large (9.0–13.0°C) degrees of subcooling below the m.p. of the polymorph ($T_p$) to crystallize directly from the melt. The β form in these model TG systems is the most stable and closely packed, whereas the α form is the least stable and most loosely packed and has a lower activation energy of formation. This means that lowering the temperature to below the α solidus line will generate the α form despite the apparently larger thermodynamic driving force for the formation of the β form.

The β and β′ polymorphs do not crystallize at the same time; indeed the formation of one polymorph seems to prevent the "competitor" polymorph from forming concurrently. This is a characteristic of the monotropic polymorphism of TG showing Ostwald's rule of stages (1). An example of this is tripalmitin at 50.5°C (see Fig. 1a). The 52.5°C experiment produces the β form after an apparent induction time of around 7 min. The β form might be expected also to appear at 50.5°C, with a shorter induction time, unless another polymorph exhausts the supply of crystallizable liquid. The β′ polymorph appears at 50.5°C, but crystallization is still in progress well past the 7-min mark, without any sign of an additional β peak, and with a substantial amount of liquid melt remaining. A small second peak does occur after 20 min at 50.5°C, which, judging from the remelt (which shows only the β form) is an exothermic transformation from β′ to β. The α and β′ polymorphs do crystallize in the same experiment but not at the same time (see Fig. 3c).

The DSC melting thermograms were used to compile a phase diagram (see Fig. 4) that is in good agreement with that produced by Lutton (11), who used a capillary melting technique. Using the DSC melting thermograms as the sole criterion for the identification of polymorphs can, however, be potentially misleading as shown by the phase diagram, where the m.p. of the β polymorph varies substantially depending on the composition of the material. The β and β′ m.p. for tristearin-rich samples can be very similar to each other in the 80–100% region of the phase diagram. When this is coupled with the variation in m.p. due to crystal imperfection, there is clear need for an additional method of crystal identification (see, for example, Fig. 2a–c). This is provided by X-ray diffraction as shown in Figure 5a for pure tripalmitin. The wide-angle X-ray diffractograms give measures of the spacing between chains, whereas diffraction maxima at the lower angles give estimates of the spacing due to the long repeat. The diffraction maximum observed at an angle of $2\theta = 6°$ has a Miller index of 003 and is consequently the third maximum due to diffraction by the lamellar planes. Substitution of the correct values in Bragg's law, $n\lambda = 2d \sin\theta$, gives a repeat of 45 Å, which corresponds to a 2-chain repeat structure. Small changes in this value for the different polymorphs reflect the degree of tilt of the chains and possibly the packing of the molecules. The traces presented in Figure 5a mimic the conditions in the DSC corresponding to Figures 3c and 3e. The α form is formed on rapid cooling (30°C $min^{-1}$ for the X-ray experiment) to a temperature of 40°C. This transforms to the β-form on heating to 55°C. Similar results are obtained for transformation from the β′-(crystallized at 45°C) to the β-forms on heating to 62°C. Identification is based on literature values (7,9,10).

*Interpolymorphic transitions.* Only limited information about interpolymorphic transitions can be obtained from the remelt—such processes are best studied using synchrotron X-ray methods. The thermograms suggest, however, that α typically undergoes melting before transforming to β, whereas β′ transforms directly to β. The observation reported by Kellens and Reynaers (13) that the β′-form is more stable in mixtures than in pure TG is also seen here in the remelting curves in Figures 2 and 3 where the pure tripalmitin and tristearin β′ form readily recrystallized to β during remelting whereas in mixtures

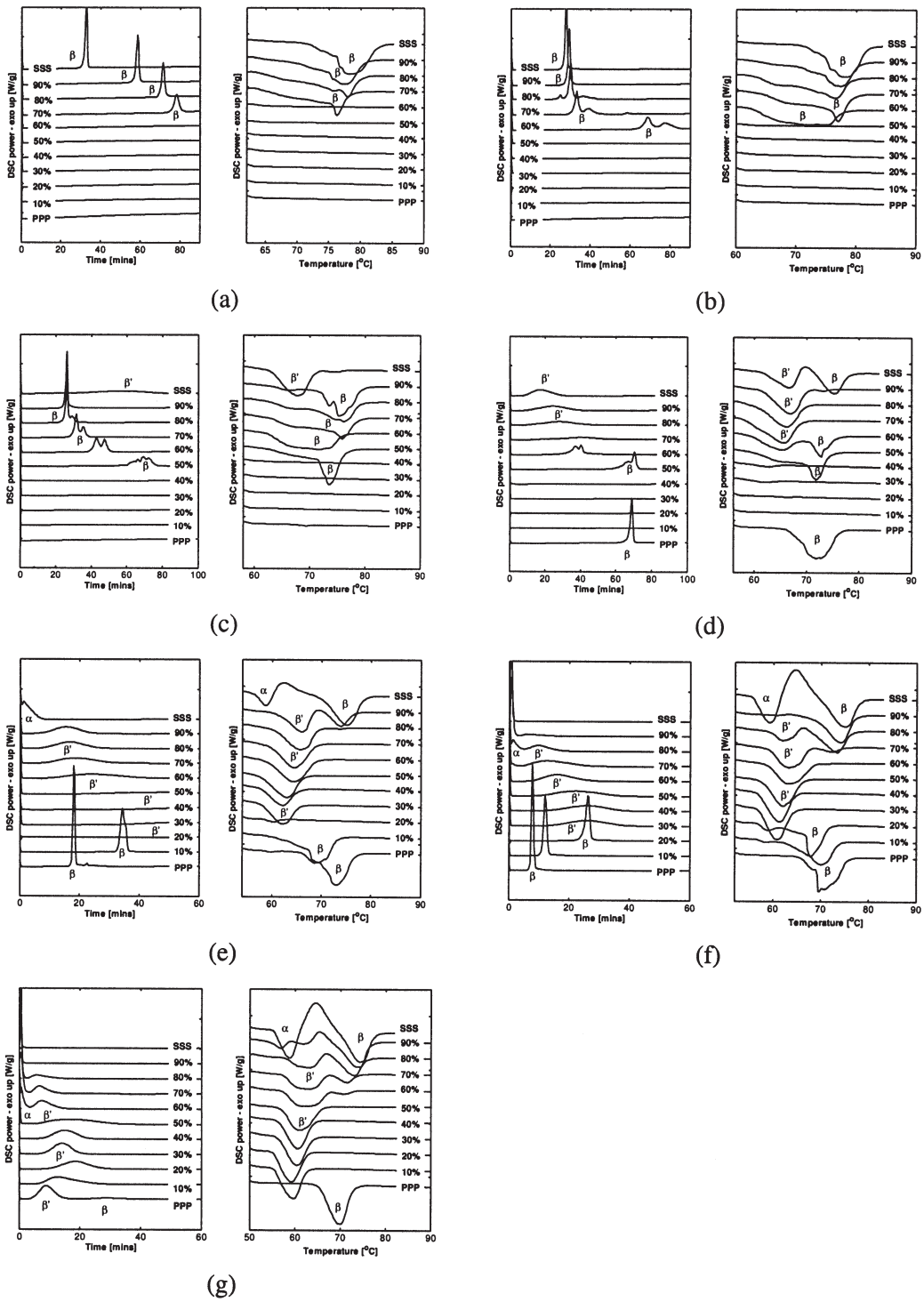


**FIG. 2.** DSC thermograms showing isothermal crystallization and melting of tripalmitin-tristearin blends (labeled as wt% tristearin) at (a) 62.5, (b) 60.5, (c) 58.5, (d) 56.5, (e) 54.5, (f) 52.5, and (g) 50.5°C. The y-axis scale divisions are 1 and 10 W/g for crystallization and remelting, respectively. The temperatures of melting for pure tripalmitin and tristearin were 65.5 and 73.5°C, respectively (11). SSS, tristearin; PPP, tripalmitin.

the β′ barely transformed at all. There is also evidence that pure tripalmitin transforms from β′ to β during the isothermal hold at 50.5°C.

*Phase separation behavior*. That β polymorphs of tripalmitin and tristearin show immiscible behavior is illustrated on the phase diagram and hinted at in Figure 2 at temperatures between 56.5 and 60.5°C, and weight fractions of 50 to 80%, where double and multiple peaks can be observed. This region is indicated by shading on the phase diagram (Fig. 4). The double peaks can be explained by the demixing of the sample into

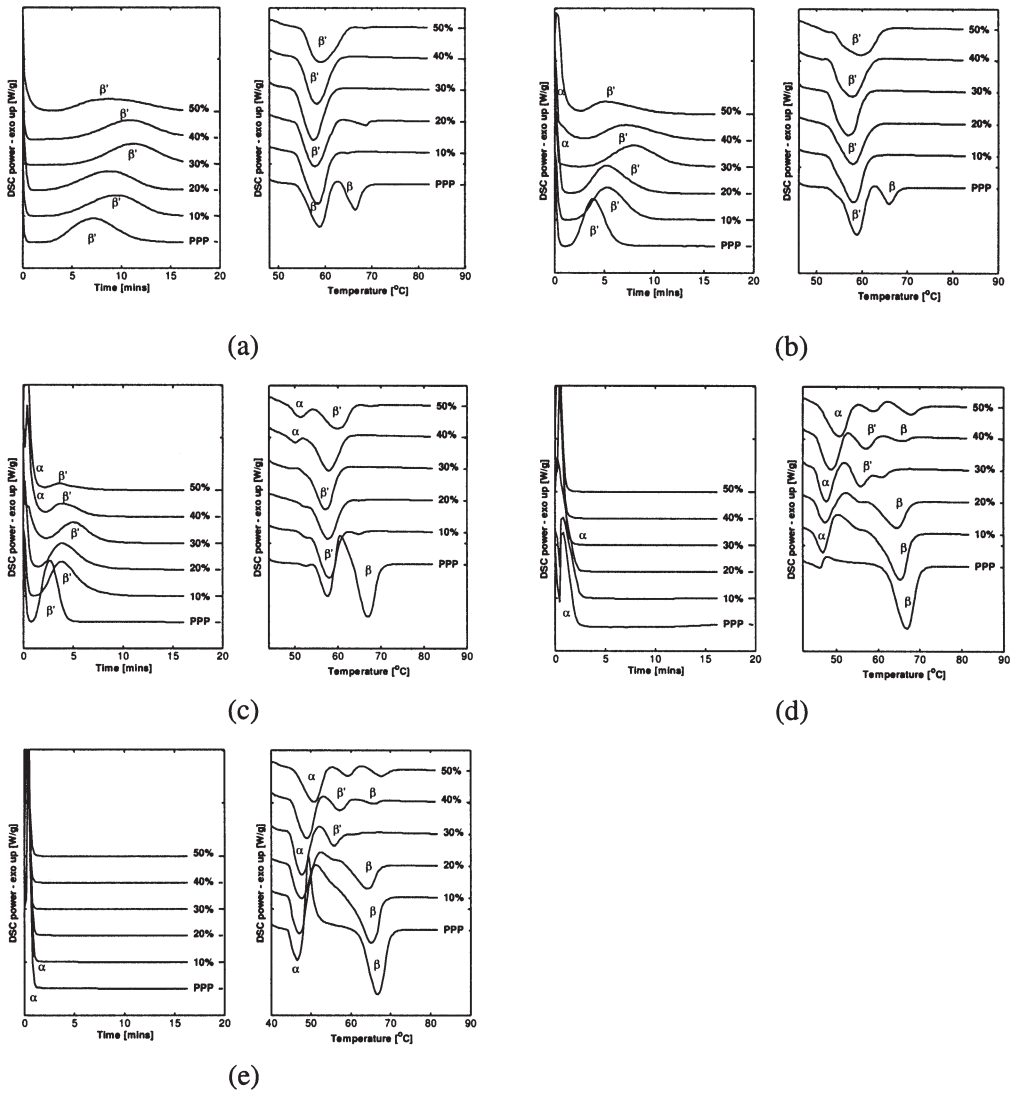


**FIG. 3.** DSC thermograms showing lower temperature isothermal crystallization and melting of tripalmitin-tristearin blends (labeled as wt% tristearin) at (a) 48.5, (b) 46.5, (c) 44.5, (d) 42.5, and (e) 40.5°C. The tripalmitin-rich region of the phase diagram was targeted in these experiments. The y-axis scale divisions are 1 and 10 W/g for crystallization and remelting thermograms, respectively. For abbreviations see Figure 2.

two separate solid β phases; one rich in tristearin and the other rich in tripalmitin. One may postulate that the tristearin-rich phase crystallizes first, which would deplete tristearin from the liquid phase. Once a sufficient concentration of tripalmitin has built up in the liquid phase, a tripalmitin-rich β phase then also crystallizes. This view is supported by the relative sizes of the first and second peaks. At constant temperature the second peak increases in area with increasing levels of tripalmitin. Confirmation of the β form is provided by X-ray diffractograms for crystallization of 60% tristearin at 58 and 60°C as shown in Figure 5b. These peaks are rather blurred owing to crystals within the samples moving out of the plane of the holder as they crystallized, but on regrinding the samples, the β form can be clearly identified as is illustrated for the 58°C reground sample.

*Fitting results*. Further analysis of crystallization kinetics was based on fitting the results to the Avrami equation (Eq. 1).

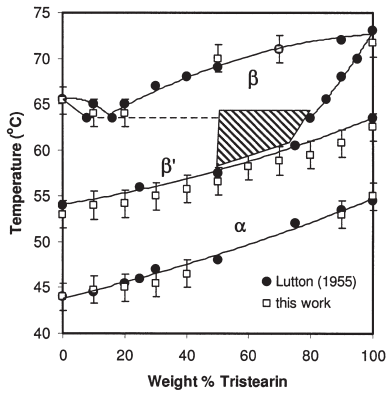


**FIG. 4.** The phase diagram of binary mixtures of tripalmitin and tristearin taken from Lutton (11) and estimated from the remelting curves in this work. Bars correspond to the uncertainty of m.p. determination of about ±1.0°C. Phase separation occurs in the shaded area; see text for details.

**TABLE 1**
**The Tripalmitin-Tristearin Composition/Temperature Matrix[a]**

| Isotherm (°C) | PPP | PPP/SSS 10% | 20% | 30% | 40% | 50% | 60% | 70% | 80% | 90% | SSS | | |
|---|---|---|---|---|---|---|---|---|---|---|---|---|---|
| 62.5 | | | | | | | | 8.6 | 9.3 | 9.8 | 10.2 | $(T_p\text{-}T)$ | [°C] |
| | | | | | | | | 3.1 | 8.1 | 6.8 | 4.9 | n | [-] |
| | | | | | | | | * 93.6 | * 139.9 | 179.5 | 189.7 | $H_{peak}$ | [kJ/kg] |
| | | | | | | | | 75.0 | 64.7 | 53.0 | 30.0 | $t_{ind}$ | [min] |
| | | | | | | | | 3.3 | 6.7 | 5.6 | 2.6 | $t_{1/2}$ | [min] |
| | | | | | | | | 6.9E-03 | 1.4E-02 | 2.4E-02 | 1.4E-02 | RMSE | [-] |
| 60.5 | | | | | | | 9.7 | 10.6 | 11.3 | 11.8 | 12.2 | $(T_p\text{-}T)$ | [°C] |
| | | | | | | | 1.8 | 1.1 | 0.9 | 6.4 | 9.9 | n | [-] |
| | | | | | | | 180.7 | 173.3 | 185.4 | 171.7 | 190.4 | $H_{peak}$ | [kJ/kg] |
| | | | | | | | 63.1 | 31.0 | 28.2 | 25.1 | 22.8 | $t_{ind}$ | [min] |
| | | | | | | | 8.4 | 3.3 | 1.9 | 4.2 | 4.8 | $t_{1/2}$ | [min] |
| | | | | | | | 3.6E-02 | 2.8E-02 | 4.5E-02 | 1.6E-02 | 7.1E-03 | RMSE | [-] |
| 58.5 | | | | | | | 11.7 | 12.6 | 13.3 | 13.8 | 5.0 | $(T_p\text{-}T)$ | [°C] |
| | | | | | | | 2.7 | 1.7 | 6.4 | 2.5 | 3.8 | n | [-] |
| | | | | | | | 181.3 | 179.1 | 181.9 | 175.5 | 170.8 | $H_{peak}$ | [kJ/kg] |
| | | | | | | | 37.1 | 28.6 | 16.6 | 24.2 | 5.5 | $t_{ind}$ | [min] |
| | | | | | | | 7.5 | 3.8 | 10.2 | 1.9 | 47.4 | $t_{1/2}$ | [min] |
| | | | | | | | 1.8E-02 | 1.7E-02 | 3.0E-02 | 2.8E-02 | 1.8E-02 | RMSE | [-] |
| 56.5 | 9.0 | | | | | 12.7 | 13.7 | 3.3 | 4.5 | 5.7 | 7.0 | $(T_p\text{-}T)$ | [°C] |
| | 7.6 | | | | | 5.4 | 4.7 | 3.0 | 2.9 | 3.2 | 2.7 | n | [-] |
| | 192.2 | | | | | 164.6 | 172.8 | 149.6 | 146.4 | 157.2 | 163.9 | $H_{peak}$ | [kJ/kg] |
| | 59.5 | | | | | 52.6 | 14.8 | 4.4 | 6.1 | 4.7 | 5.3 | $t_{ind}$ | [min] |
| | 4.9 | | | | | 15.6 | 23.3 | 35.1 | 22.6 | 19.7 | 11.3 | $t_{1/2}$ | [min] |
| | 2.5E-02 | | | | | 2.5E-02 | 2.6E-02 | 8.4E-03 | 3.3E-03 | 8.9E-04 | 2.1E-03 | RMSE | [-] |
| 54.5 | 11.0 | 10.5 | | | | 3.3 | 4.3 | 5.3 | 6.5 | 7.7 | 0.3 | $(T_p\text{-}T)$ | [°C] |
| | 3.5 | 7.1 | | | | 3.8 | 2.5 | 2.3 | 2.8 | 2.9 | | n | [-] |
| | 172.9 | 184.8 | | | | * 45.0 | 151.7 | 155.4 | 144.9 | 147.7 | | $H_{peak}$ | [kJ/kg] |
| | 17.1 | 29.1 | | | | 13.3 | 8.5 | 7.0 | 5.6 | 4.6 | | $t_{ind}$ | [min] |
| | 1.1 | 5.5 | | | | 29.8 | 17.2 | 13.1 | 11.2 | 11.4 | | $t_{1/2}$ | [min] |
| | 4.7E-03 | 1.2E-02 | | | | 9.1E-03 | 8.7E-04 | 3.7E-03 | 3.3E-03 | 4.8E-03 | | RMSE | [-] |
| 52.5 | 13.0 | 12.5 | 9.5 | 3.6 | 4.4 | 5.3 | 6.3 | -1.5 | -0.3 | 1.0 | 2.3 | $(T_p\text{-}T)$ | [°C] |
| | 2.8 | 2.3 | 7.9 | 3.4 | 3.5 | 2.7 | 2.3 | | | | | n | [-] |
| | 188.9 | 183.2 | 162.5 | 162.8 | 166.6 | 159.6 | 151.8 | | | | | $H_{peak}$ | [kJ/kg] |
| | 6.9 | 10.7 | 19.0 | 8.8 | 6.7 | 7.5 | 7.2 | | | | | $t_{ind}$ | [min] |
| | 1.0 | 1.4 | 7.2 | 17.3 | 19.4 | 16.2 | 9.2 | | | | | $t_{1/2}$ | [min] |
| | 1.2E-02 | 1.8E-02 | 2.2E-02 | 3.5E-03 | 2.9E-03 | 1.2E-03 | 4.2E-03 | | | | | RMSE | [-] |
| 50.5 | 3.6 | 4.2 | 4.8 | 5.6 | 6.4 | 7.3 | -0.7 | 0.5 | 1.7 | 3.0 | 4.3 | $(T_p\text{-}T)$ | [°C] |
| | 2.6 | 1.8 | 2.7 | 3.3 | 3.1 | 2.5 | | | | | | n | [-] |
| | 154.9 | 160.4 | 146.4 | 159.4 | 157.5 | 146.8 | | | | | | $H_{peak}$ | [kJ/kg] |
| | 3.8 | 5.6 | 5.3 | 3.9 | 6.9 | 4.9 | | | | | | $t_{ind}$ | [min] |
| | 5.3 | 8.2 | 9.9 | 8.6 | 9.9 | 13.7 | | | | | | $t_{1/2}$ | [min] |
| | 3.4E-03 | 4.4E-03 | 4.6E-03 | 3.4E-03 | 2.4E-03 | 3.2E-03 | | | | | | RMSE | [-] |
| 48.5 | 5.6 | 6.2 | 6.8 | 7.6 | 8.4 | 0.2 | 1.3 | 2.5 | 3.7 | 5.0 | | $(T_p\text{-}T)$ | [°C] |
| | 2.7 | 3.3 | 3.8 | 1.9 | 2.0 | | | | | | | n | [-] |
| | 154.6 | 156.7 | 140.9 | 149.7 | 138.3 | | | | | | | $H_{peak}$ | [kJ/kg] |
| | 1.8 | 3.1 | 3.8 | 5.4 | 4.2 | | | | | | | $t_{ind}$ | [min] |
| | 3.0 | 4.8 | 7.2 | 5.3 | 7.4 | | | | | | | $t_{1/2}$ | [min] |
| | 2.8E-03 | 3.4E-03 | 3.5E-03 | 8.8E-03 | 3.1E-03 | | | | | | | RMSE | [-] |

β

double-peak

β

β'

α

[a]Values of crystallization driving force, $(T_p - T)$; parameter $n$; peak enthalpy, $H_{peak}$; induction time, $t_{ind}$; time to half crystallization, $t_{1/2}$; and RMSE, root mean square of error. The polymorphic forms that crystallized are also indicated with groupings of polymorphs delineated by bold lines. *Isothermal thermograms are not complete.

It should be noted that the Avrami equation is meant to model single crystallization events only, and therefore incidences where multiple peaks or interpolymorphic transitions occurred are unlikely to be well-fitted. In general, the Avrami equation provided better fits to the β′ crystallization data compared with β, as shown by an order-of-magnitude lower values of RMSE. The values of $n$ for crystallization lie, in many cases, beyond the physical basis of the Avrami model ($n > 4$) which is not the case for β′ crystallization ($1.8 < n < 3.8$). High crystallization driving forces $(T_p - T)$ for β cause high nucleation and growth

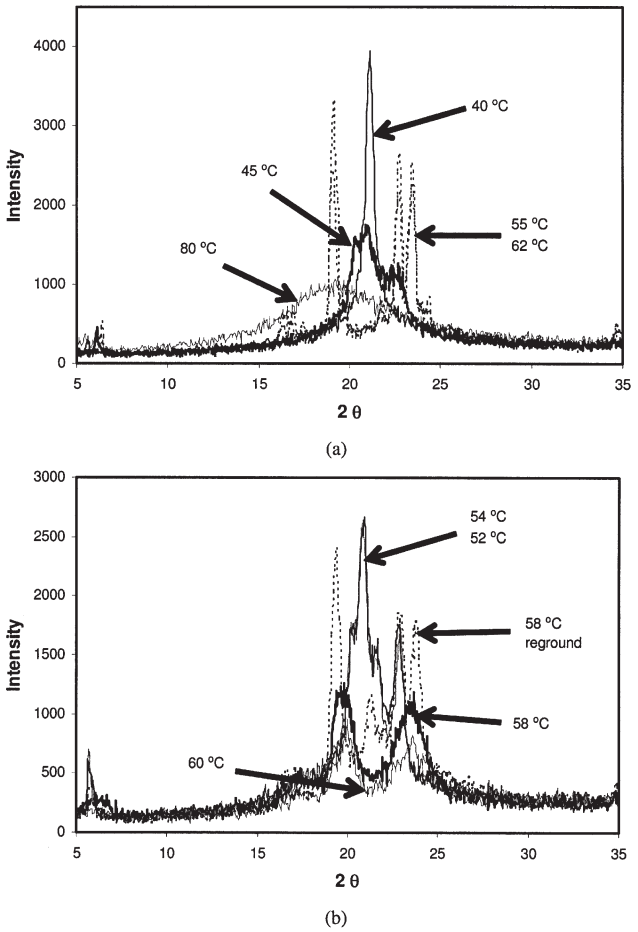


**FIG. 5.** X-ray diffractograms corresponding to (a) the pure tripalmitin traces of Figure 3c and 3e. Heat to 80°C (melt), cool to 40°C (α-form), and heat to 55°C (β-form); heat to 80°C (liquid), cool to 45°C (β′-form), and heat to 62°C (β-form); (b) the 60% tristearin blend showing crystallization of β′-form at 52 and 54°C and β-form at 58 and 60°C. The peaks are rather blurred because of crystals within samples moving out of the plane of the holder as they solidified. The reground sample peaks clearly indicate the β polymorph.

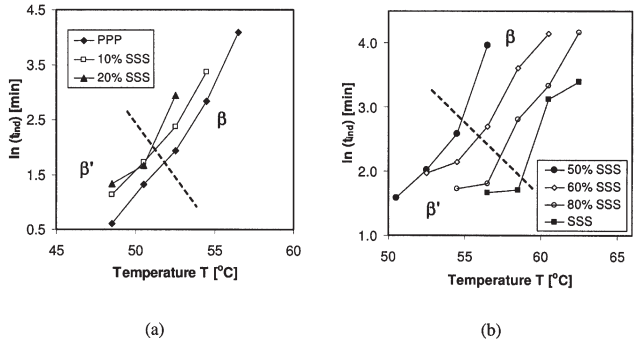


**FIG. 6.** Plots of $\ln(t_{ind})$ against isothermal temperature for β′- and β-forms of (a) tripalmitin-rich mixtures and (b) tristearin-rich mixtures, showing shorter induction times where one species predominates. $t_{ind}$, apparent induction time; for other abbreviations see Figure 2.

rates (revealed in very sharp peaks) as well as long apparent induction times (in many cases >30 min), causing greater fitting errors.

Reproducibility tests were performed for the following combinations of composition and isothermal hold temperature: (i) 60% tristearin (SSS) at 54.5°C (a "flat" β′ exotherm), (ii) 90% SSS at 54.5°C (a less flat β′ exotherm), (iii) 90% SSS at 58.5°C (a β exotherm), and (iv) pure SSS at 62.5°C (a β exotherm with a longer induction time). SD values for $t_{ind}$ and $t_{1/2}$ were all less than 1 min with the exception of $t_{1/2}$ for 90% SSS at 54.5°C (SD of 1.5 min) and $t_{ind}$ for pure SSS at 62.5°C (SD of 11.1 min). Therefore, fitted time values can be treated with a reasonable degree of confidence with the exception of $t_{ind}$ for longer induction times. SD for peak enthalpy values were 2.9, 3.7, 5.5, and 5.8 kJ/kg for samples (a), (b), (c), and (d) respectively, thus slightly higher for the two β exotherms than the β′ exotherms.

Figures 6a and 6b summarize the apparent induction times extracted from the data of Figures 1, 2, and 3 for β′- and β-forms. Apparent induction times for the α-form are too short to be recorded reliably and are not shown in the figures. At a given temperature the apparent induction times are generally longest for samples at an intermediate composition and shortest where one species predominates. It was found that for all samples of a given composition, apparent induction times decreased with decreasing temperature. Interestingly, although the apparent induction time data plotted in Figure 6 fall into different areas of the plot depending on the polymorph produced, there appears to be little sign of any discontinuity in value in the trend of apparent induction time with temperature arising from changes in polymorph, although the slopes look noticeably different. One hypothesis that might explain this observation is that the polymorphic form that arises is simply determined by which polymorph is able to nucleate first. If so, the crossover point between polymorphs on Figure 6 would by definition occur at the point where the induction times of the two polymorphs are equal.

A different perspective is provided from estimations of the activation free energy for nucleation of β′- and β-forms from

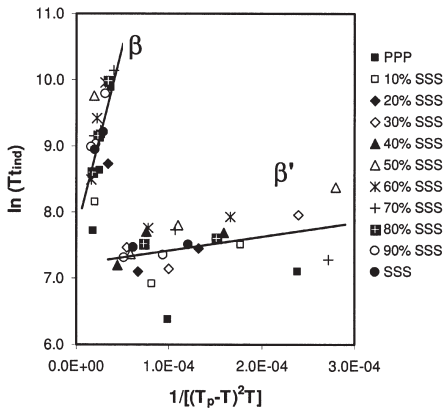


**FIG. 7.** A plot of $\ln(Tt_{ind})$ against $1/[(T_p - T)^2 T]$ for all mixtures showing a higher slope for the β-form (56,500 $K^{-3}$) compared with the β′-form (2,090 $K^{-3}$). The units used are minutes for $t_{ind}$ and Kelvin for temperature, $T$. For other abbreviations see Figure 2.

**TABLE 2**
**Calculated Values for $\Delta G_{cryst}$ (kJ/mol) of β′- and β-Forms[a]**

| Isotherm (°C) | PPP | PPP/SSS | | | | | | | | | SSS |
|---|---|---|---|---|---|---|---|---|---|---|---|
| | | 10% | 20% | 30% | 40% | 50% | 60% | 70% | 80% | 90% | |
| 62.5 | β | | | | | β | | 6.31 | 5.40 | 4.86 | 4.56 |
| 60.5 | | | | | | | 4.95 | 4.16 | 3.66 | 3.35 | 3.18 |
| 58.5 | | | | | | double peak | 3.41 | 2.94 | 2.64 | 2.45 | 0.70 |
| 56.5 | 5.80 | | | | | 2.93 | 2.49 | 1.56 | 0.87 | 0.54 | 0.36 |
| 54.5 | 3.88 | 4.26 | | | | 1.60 | 0.95 | 0.61 | 0.41 | 0.29 | |
| 52.5 | 2.78 | 3.01 | 5.20 | 1.36 | 0.90 | 0.62 | 0.44 | β′ | | | |
| 50.5 | 1.34 | 1.00 | 0.74 | 0.56 | 0.42 | 0.33 | | | | | |
| 48.5 | 0.56 | 0.46 | 0.37 | 0.30 | 0.25 | | | | | | |

[a]Calculated using Equation 5 (see text) and with the slope values for each polymorph taken from the regression fits in Figure 7 and the values of $(T_p - T)$ from Table 1.

plots of $\ln(Tt_{ind})$ against $1/[(T_p - T)^2T]$ (see Eqs. 3–5), which are shown on Figure 7. Good linear correlations are obtained for both β′- and β-forms with little apparent dependence on composition. It can be seen that a much larger slope results for the β polymorph (56,500 $K^{-3}$) compared with β′ (2,090 $K^{-3}$). These slopes have been used to generate values of activation free energy of nucleation for each sample condition according to Equation 5, and these are shown in Table 2. The activation free energies values derived are still higher for β than for β′ despite the higher denominator terms for β in Equation 5. This is in line with the well-established view that β polymorph nucleation is more difficult to initiate (has a larger energy barrier) than β′.

*Peak widths and the $t_{1/2}$ of β′- and β-forms.* The crystallization exotherms for the formation of β polymorphs are much sharper than for β′ and consequently have shorter $t_{1/2}$ values. This indicates that, once initiated, the crystallization of β proceeds at a much higher rate than that of β′, suggesting faster crystal growth kinetics. Figure 8a suggests that this is principally due to the larger driving force $(T_p - T)$ required to initiate β crystallization.

At a given temperature, $t_{1/2}$ times also are generally longest for samples at an intermediate composition and shortest where one species predominates. This is observed for both β and β′ forms. This composition effect has been similarly observed by Taran *et al.* (21) for simple eutectic-forming binary melts. On the tristearin-rich side of the eutectic composition, this is explained by a lower crystallization driving force as more tripalmitin is added, due to the tripalmitin lowering the melting temperature of the tristearin as shown on Figure 8a. When this is taken into account, there is no clear dependence on composition. However, this argument cannot be used for the tripalmitin-rich side of the eutectic. As tristearin is added, as shown in Figure 8b, $t_{1/2}$ increases significantly compared with pure tripalmitin, for the same driving force $(T_p - T)$. A more likely explanation is a greater mass transfer resistance when each TG is present. This could be caused either by difficulties in penetrating through a depletion layer, as one species diffuses through the other, or in the surface integration step, where one species disrupts the crystal packing of the other. However, this only appears to occur in the tripalmitin-rich side of the eutectic composition.

*The kinetics of α polymorph crystallization.* The crystallization of the α form is so rapid that it is generally difficult to deconvolute from the cooling step (Fig. 3, 40.5 and 42.5°C). No kinetic analysis was undertaken, although it can be seen in Figure 3d that

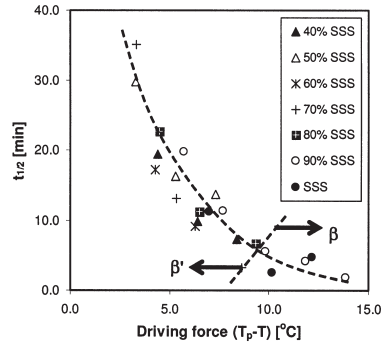


(a)

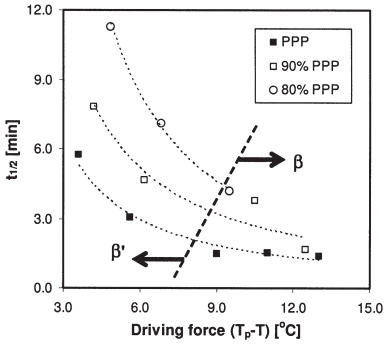


(b)

**FIG. 8.** (a) Plot of $t_{1/2}$ against crystallization driving force $(T_p - T)$ for tristearin concentrations higher than the eutectic composition, i.e., to the right of the eutectic point ("double peak" data are excluded). The effect of driving force is dominant in determining the crystallization rates. (b) A similar plot for mixtures with lower tristearin concentrations than the eutectic composition. In this region there is a significant effect of composition on the crystallization rates in addition to the driving force. $t_{1/2}$, time for half of the overall level of crystallization to be reached after $t_{ind}$ has passed; for other abbreviations see Figures 2, 6, and 7.

α crystallization is slightly faster than β crystallization. However, as with the β′ process, the main reason for the overall rapidity of the crystallization is the much reduced induction time. One approach to extract the kinetics will be to use nonisothermal crystallization methods (22).

## ACKNOWLEDGMENT

We wish to acknowledge and thank the Biotechnology and Biological Sciences Research Council (Swindon, United Kingdom) for funding this work (grant reference D20450).

## REFERENCES

1. Sato, K., and N. Garti, *Crystallization Processes in Fats and Lipid Systems*, Marcel Dekker, New York, 2001.
2. Timms, R.E., Phase-Behaviour of Fats and Their Mixtures, *Prog. Lipid Res. 23*:1–38 (1984).
3. Wesdorp, L.H., Liquid-Multiple Solid-Phase Equilibria in Fats—Theory and Experiments, Ph.D. Thesis, Delft University of Technology, The Netherlands, 1990.
4. Minato, A., S. Ueno, K. Smith, Y. Amemiya, and K. Sato, Thermodynamic and Kinetic Study on Phase Behavior of Binary Mixtures of POP and PPO Forming Molecular Compound Systems, *J. Phys. Chem. B. 101*:3498–3505 (1997).
5. Rousset, P., M. Rappaz, and E. Minner, Polymorphism and Solidification Kinetics of the Binary System POS–SOS, *J. Am. Oil Chem. Soc. 75*:857–864 (1998).
6. Sato, K., and T. Kuroda, Kinetics of Melt Crystallization and Transformation of Tripalmitn Polymorphs, *Ibid. 64*:124–127 (1987).
7. Kellens, M., W. Meeussen, and H. Reynaers, Study of the Polymorphism and the Crystallization Kinetics of Tripalmitin—A Microscopic Approach, *Ibid. 69*:906–911 (1992).
8. Kellens, M., and H. Reynaers, Study of the Polymorphism of Saturated Monoacid Triglycerides I. Melting and Crystallization Behavior of Tristearin, *Fat Sci. Technol. 94*:94–100 (1992).
9. Kellens, M., W. Meeussen, C. Riekel, and H. Reynaers, Time Resolved X-ray Diffraction Studies of the Polymorphic Behaviour of Tripalmitin Using Synchrotron Radiation, *Chem. Phys. Lipids. 52*:79–98 (1990).
10. Kellens, M., W. Meeussen, and H. Reynaers, Crystallization and Phase Transition Studies of Tripalmitin, *Ibid. 55*:163–178 (1990).
11. Lutton, E.S., Phase Behavior of Triglyceride Mixtures Involving Primarily Tristearin, 2-Oleyldistearin and Triolein, *J. Am. Oil Chem. Soc. 32*:49–53 (1955).
12. Cebula, D.J., and P.R. Smith, Dynamic Polymorphic Phase Transitions in a Model Binary Triglyceride System Measured by Position-Sensitive X-Ray Diffraction Methods, *Ibid. 67*(11):811–814 (1990).
13. Kellens, M., and H. Reynaers, Study of the Polymorphism of Saturated Monoacid Triglycerides II. Polymorphic Behavior of a 50/50 Mixture of Tripalmitin and Tristearin, *Fat Sci. Technol. 94*:286–293 (1992).
14. Eads, T.M., A.E. Blaurock, R.G. Bryant, D.J. Roy, and W.R. Croasman, Molecular Motion and Transitions in Solid Tripalmitin Measured by Deuterium Nuclear Magnetic Resonance, *J. Am. Oil Chem. Soc. 69*:1057–1068 (1992).
15. Sato, K., S. Ueno, and J. Yano, Molecular Interactions and Kinetic Properties of Fats, *Prog. Lipid Res. 38*:91–116 (1999).
16. McNaughton, J.L., C.T. Mortimer, *Differential Scanning Calorimetry IRS* Physical Chemistry Series 2, Vol. 10, Butterworths, London, 1975.
17. Avrami, M., Kinetics of Phase Change I. General Theory, *J. Chem. Phys. 7*:1103–1112 (1939).
18. Avrami, M., Kinetics of Phase Change II. Transformation–Time Relation for Random Distribution of Nuclei, *Ibid. 8*:212–224 (1940).
19. Turnbull, D., and J.C. Fisher, Rate of Nucleation in Condensed Systems, *Ibid. 17*:71–73 (1949).
20. Ng, W.L., A Study of the Kinetics of Nucleation in a Palm Oil Melt, *J. Am. Oil Chem. Soc. 67*:879–882 (1990).
21. Taran, A.L., G.A. Nosov, S.K. Myasnikov, and A.Y. Kholin, Kinetics of Crystallization of Binary Melts of Eutectic-Forming Substances, *Theor. Found. Chem. Eng. 38*:164–168 (2004).
22. Smith, K.W., F.W. Cain, and G. Talbot, Kinetic Analysis of Nonisothermal Differential Scanning Calorimetry of 1,3-Dipalmitoyl-2-oleoylglycerol, *J. Agric. Food Chem. 53*:3031–3040 (2005).

[Received June 16, 2005; accepted November 1, 2005]